Current Science International
ISSN 2077-4435

Volume : 04 | Issue : 04| Oct.-Dec.|2015
Pages**:** 658-667

Finite Element Analysis of Spun Concrete Poles Reinforced with Glass Fiber Reinforced Polymer (GFRP) Bars

Ashraf M. Shalaby

Civil Engineering Department, National Research Centre, Dokki, Giza, Egypt

ABSTRACT

This paper focus on modeling the flexural behavior of spun concrete poles reinforced with GFRP bars using finite element analysis. The finite element model was then verified through comparing the results with the results available in the literature. Two poles were modeled using the ANSYS software. The poles were identical to each other, and the only difference was in the number of GFRP bars, one pole having 6 bars and the other 12. Poles were tapered with 20ft (6.1m) long. The results of this paper show that the finite element model used in this study shows a good correlation with the experimental results, and can be used for further studies of spun concrete poles reinforced with GFRP bars.

Key words: Concrete Poles; Glass Fiber Reinforced Polymers; GFRP; Finite Element Analysis, ANSYS

Introduction

Finite element modeling of concrete structures is a very useful research tool that helps in understanding the behavior of the structure prior to loading, and it has been widely spread especially after the advancement in the computer software and computational methods. Moreover, finite element analysis can help in decreasing the number of specimens required for testing, and as a result decrease the all-in-all budget of the research project.

Spun concrete poles reinforced with GFRP bars are a new alternative to traditional prestressed spun concrete poles that are primarily used for supporting electric power transmission lines and distribution and for area lighting. Unlike traditional concrete poles, spun concrete poles reinforced with GFRP bars can be installed in aggressive environments, such as brackish or salt water without being afraid of deterioration due to corrosion of the steel reinforcement since they are reinforced using GFRP bars. GFRP bars provide an excellent alternative to steel reinforcement due to their corrosion resistance and durability.

This paper presents the modeling of spun concrete poles reinforced with GFRP bars using the commercially available finite element software (ANSYS, 2015); the model is then verified using experimental data.

Finite Element Model

Modeling of concrete poles using finite element software involves defining the element types and material properties used to model the concrete and the GFRP reinforcement. This section discusses the two element types used to model the concrete and GFRP reinforcement, and presents the mechanical properties of concrete and GFRP that were used in the model.

Element Types

SOLID65 of the ANSYS software was used to model the concrete. This solid element has eight nodes with three degrees of freedom at each node. Each node can accept translational movement in the x, y, and z directions, but none of them can accept rotational movement. This element was designed by ANSYS especially to model concrete structures, as it is capable of crushing in compression, cracking in tension, and plastic deformation.

Link180 of the ANSYS software was used to model the GFRP reinforcement; this is a 3D element that has two nodes with three degrees of freedom at each node. Each node can accept translational movement in the x, y, and z directions.

Real Constants

Real constants are used by ANSYS to input the data that are required for the calculation of the element matrix but cannot be determined from the node locations or material properties. Typical real constants include area, thickness, inner diameter, and outer diameter.

Corresponding Author: Ashraf M. Shalaby, Civil Engineering Department, National Research Centre, Dokki, Giza, Egypt
E-mail: shalaby.ashraf@gmail.com

Real constant set 1 is used for the Solid 65 element. It requires real constants for rebar, assuming a smeared model. Values can be entered for material number, volume ratio, and orientation angles. The material number refers to the type of material for the reinforcement. The volume ratio refers to the ratio of steel to concrete in the element. The orientation angles refer to the orientation of the reinforcement in the smeared model.

ANSYS allows the user to enter three rebar materials in the concrete. Each material corresponds to x, y, and z directions in the element. The reinforcement has uniaxial stiffness, and the directional orientation is defined by the user. In the present study, the poles were modeled using discrete reinforcement; therefore, a value of zero was entered for all real constants, which turned off the smeared reinforcement capability of the solid 65 element off.

Real constant set 2 was defined for the Link180 element. Values for the cross-sectional area of the GFRP bars and initial strain were entered. A value of zero was entered for the initial strain, because there was no initial strain applied to the GFRP reinforcement. Real constants for Link180 are shown in Table 1.

Table 1: Real constants for Link8 element

Real Constants	
Cross-sectional Area (in^2)	0.101
Initial Strain	0

Note: $1in^2 = 645\ mm^2$

Material Properties

The materials used in this study were the concrete and the GFRP reinforcement. For reinforced concrete structures, the material properties are defined by the compressive and tensile strengths, and by the modulus of elasticity of the material.

Concrete

The concrete used in this study was a specially formulated, high strength concrete mix for spun concrete poles designed and produced by the batch plant. This mixture was designed to produce a concrete with an average compressive strength of about 11,000 psi (75.84 MPa) at 28 days (Table 2). Different equations have been used to calculate the elastic modulus of concrete; however it was found by Nunez (2002) that the equation used by Nawy, (2000) falls within the upper and lower bound expressions for the estimation of modulus of elasticity, therefore, it was used in this study. The modulus of elasticity of concrete is calculated as follows:

$$E_c(psi) = \left[40000\sqrt{f_c^{'}} + 10^6\right]\left(\frac{w}{145}\right)^{1.5}$$

Where, $f_c^{'}$ is the average compressive strength of concrete at 28 days, w is the unit weight of concrete in lb/in^3.

In concrete with normal compressive strength and up to strength of 6000 psi the peak strain ε_0 in compression is equal to 0.002; however, for high strength concrete, the peak strain in compression was calculated as follows (Nunez, 2002):

$$\varepsilon_0 = 0.001306 + 1.3789 \times 10^{-7} f_c^{'}$$

The following equations2 were used to construct the uniaxial compressive stress strain curve for concrete in this study:

$$f = \frac{f_c^{'} \beta \left(\frac{\varepsilon}{\varepsilon_0}\right)}{\beta - 1 + \left(\frac{\varepsilon}{\varepsilon_0}\right)^{\beta}}$$

$$\beta = \frac{1}{1 - \frac{f_c'}{\varepsilon_0 E_0}}$$

Where, f is the stress at any strain ε, and ε is the strain at any stress f. Figure 1 shows the stress strain curve constructed using the above equations.

Table 2: Summary of Material Properties for Concrete

Modulus of Elasticity, E_c (psi)	Peak Strain, ε_0	Compressive Strength, f_c' (psi)	Tensile Strength, f_r (psi)	Poisson's Ratio, ν
5195235	0.00282	11000	585	0.25

Note: 1000 psi = 6.89 MPa

ANSYS software uses the smeared crack approach (Willam and Warnke, (1974), to model the cracks in concrete, which requires the definition of a number of constants. These constants are the shear transfer coefficient, the uniaxial tensile cracking stress, and the uniaxial crushing stress. The shear transfer coefficient range from a value of 0 to 1.0, with zero representing a smooth crack and 1.0 representing a rough crack. As reported by Kachlakev *et al.* (2001), the value of the shear transfer coefficient for open cracks varied between 0.05 and 0.25. In this study, a number of preliminary analyses were tried with different values for the shear transfer coefficient within this range, and a value of 0.125 was used, as it was able to closely predict the behavior of the poles. The uniaxial tensile stress was entered as per the experimental records. Although it was recommended by previous research (Kachlakev *et al.,* 2001; Barbosa and Ribeiro, 1998) to disable the uniaxial crushing stress capability, it was entered as per the theoretical records to study its effect on the model. Poisson's ratio for concrete was assumed to be 0.25. Table 2 shows a summary of the concrete properties.

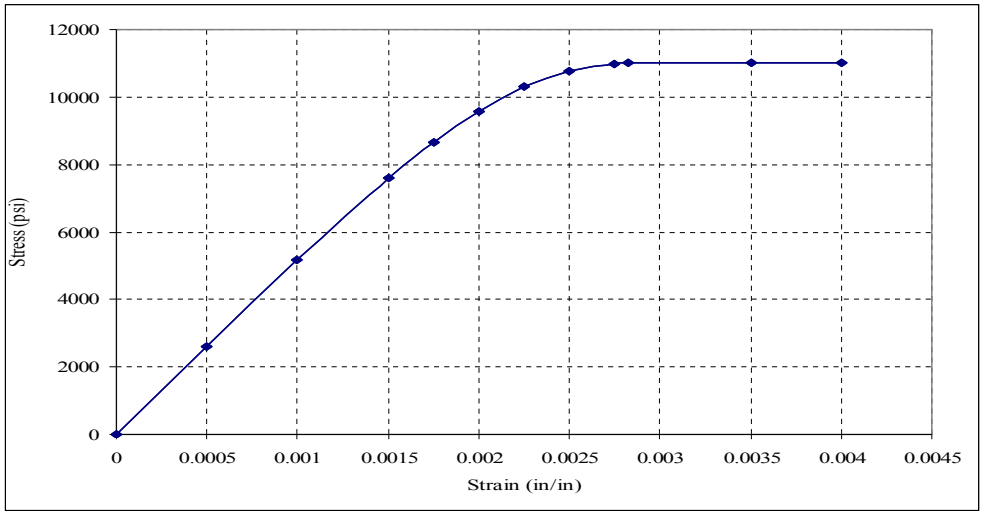

Fig. 1: Concrete stress-strain curve adopted in the FE model
Note: 1in = 25.4 mm 1000 psi = 6.89 MPa

GFRP Bars

The GFRP bars used in this study were provided by Hughes Brothers Inc., and its physical properties are listed in Table 3. GFRP behaves linearly up to failure and was modeled as a linear elastic material.

Table 3: Physical Properties of GFRP

Bar Dia. (in)	Cross-Sectional Area (in^2)	Nominal Diameter (in)	Tensile Strength (ksi)	Tensile Modulus of Elasticity (psi 10^6)	Ultimate Strain (%)
#4	0.196	0.50	100	5.92	1.7

Note: 1in = 25.4 mm *$1in^2 = 645\ mm^2$* *1000 psi = 6.89 MPa*

Structure Modeling

Two poles were modeled using the ANSYS software. The poles were identical to each other, and the only difference was in the number of GFRP bars, one pole having 6 bars and the other 12. Poles were 20ft (6.1m) long, with an outside slope of 1.8% making an outer diameter of 8.91 in (226 mm) and 13.23 in (336 mm) at tip and butt ends, respectively. The inner diameters were 3.91 in (99.3 mm) and 7.75 in (191 mm) for the tip and but ends respectively, with an inside slope of 1.6%. The wall thickness was 2.5 in (64 mm) and 2.74 in (69.6 mm) at the tip and butt ends, respectively.

The poles were modeled using the volume option and meshed using the volume sweep option. The mesh size was based on a convergence study that was performed to determine a suitable mesh. The poles were meshed every 2 in (50 mm) in the longitudinal direction (Figure 2), and in the cross-section they were meshed on an angle of 15º, as shown in Figure 3. Figure 3 also shows the orientation of the GFRP bars in the cross-section. The figure shows that the 6 GFRP bars of the first pole were not symmetrically distributed around the cross-section. The 6 GFRP bars were modeled that way to match with the orientation of the actual test specimens. The pole with the 6 GFRP bars were oriented in the actual test specimens as shown in Figure 3 because they were restricted by the available opening in the end plates of the molds where the poles were cast. GFRP bars were added to the model, as Link180 element, so that they share the same nodes for concrete (Figure 4), assuming a perfect bond. Each GFRP bar was divided into 120 Link180 elements, so that each element was 2 in (50 mm) long. A preliminary run was tried to check the effect of the stirrups on the results and was found to be not significant, so they were left out in order to decrease the number of elements and perform faster computations. Both finite element models had 5760 Solid65 elements. The first model where the pole was reinforced with six bars had 720 Link180 elements, and the second model where the pole was reinforced with 12 bars had 1440 Link180 elements.

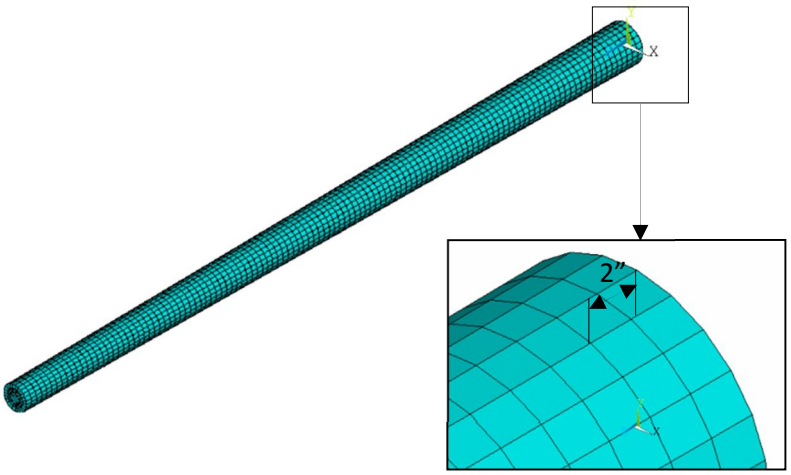

Fig. 2: Finite Element Meshing of the Pole in the Longitudinal Direction
Note: 1in = 25.4 mm

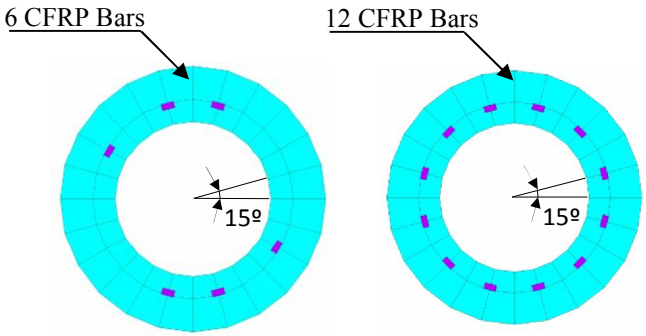

Fig. 3: Finite Element Meshing of the Pole in the Cross-sectional Direction

Loads and Boundary Conditions

Displacement boundary conditions are needed to constrain the model to get a reliable solution for stresses and deformations. Two types of boundary conditions were applied, one was to model the support condition of the poles and the second was to prevent any out-of-plane displacements that might affect the results. The first set of boundary conditions was applied at two locations, one at the butt end of the pole and the other at 3.00 ft (1000 mm) from the butt end. These distances were chosen to match the experimental test setup. The supports were modeled as fixed supports, so the displacement in all three directions was prevented, and since the poles were modeled as solid elements, therefore, by constraining the displacement at two nodes of the elements, the rotation will be prevented. The second set of boundary conditions was applied to all of the nodes. All of the nodes were prevented from displacement in the out-of-plane direction by constraining the displacement in the x-direction (Figure 5).

During the test, the load was applied at a distance of 1.0 ft (305 mm) from the tip of the pole using a strap that surrounded half the circumference of the pole and connected to the chain hoist. In order to match the test setup in our model, the load was also applied at 1.0 ft (305 mm) from the tip end of the pole as point loads over the nodes covering half the circumference of the cross-section, as shown in Figure 6. Another reason for distributing the load over the nodes at this section is that if the load was applied on only one node, distortion to the elements connected to this node would happen and the file would not run. The load applied at each node was equal to one over thirteen of the actual load applied.

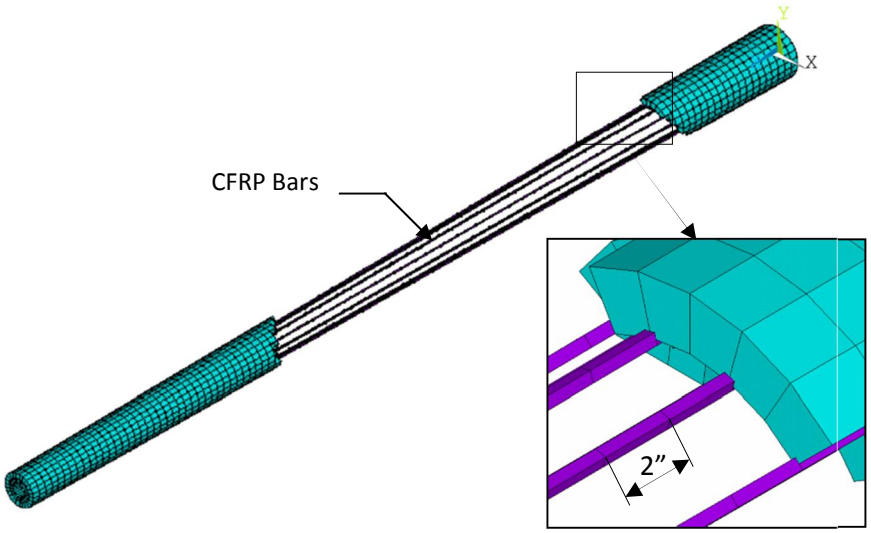

Fig. 4: Finite Element Modeling of the CFRP Bars
Note: 1in = 25.4 mm

Analysis Type

The finite element model for this analysis was a cantilever pole under point loading. For the purpose of this model, the static analysis type was used. The solution control commands incorporated by the ANSYS and used to perform this analysis is discussed below.

The Newton-Raphson method

- The Newton-Raphson method incorporated by the ANSYS was used to compute the nonlinear response. Using this method, the load was subdivided into a series of load increments, and the load increments were applied over several load steps. As per the ANSYS manual, the Newton-Raphson method can be described as follows.

Before each solution, the Newton-Raphson method evaluates the out-of-balance load vector, which is the difference between the restoring forces (the loads corresponding to the element stresses) and the applied loads. The program then performs a linear solution, using the out-of-balance loads, and checks for convergence. If the convergence criteria are not satisfied, the out-of-balance load vector is reevaluated, the stiffness matrix is

updated, and a new solution is obtained. This iterative procedure continues until the problem converges (ANSYS, 2015) .

Loads were applied in very small increments that sometimes reached 1 lb (0.45 kN) to avoid any convergence problems that might occur and to fulfill the requirements of the Newton-Raphson method.

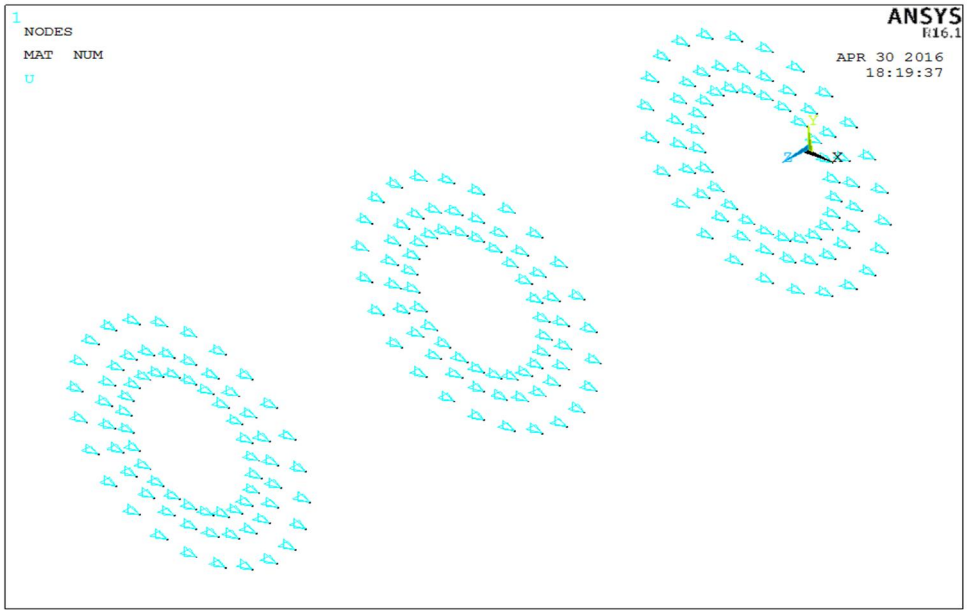

Fig. 5: Sample of the out-of-plane joint restraints

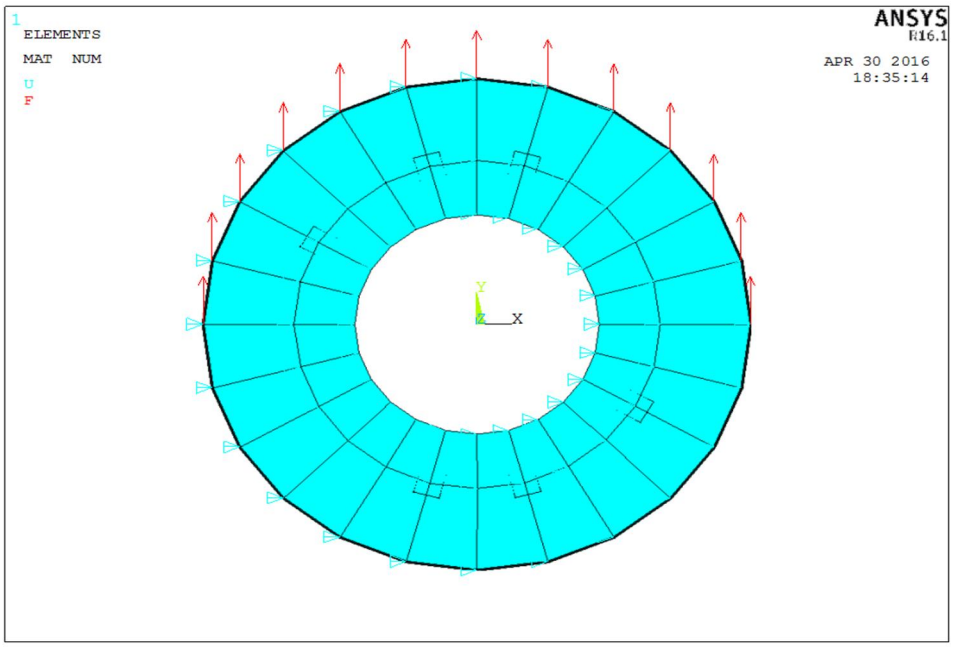

Fig. 6: Point loads applied to the pole

Equation solvers

- ANSYS incorporates several methods of solving simultaneous equations; however, the sparse direct solver is the default for most of the analyses. The sparse direct solver is based on a direct elimination of equations, as opposed to iterative solvers, where the solution is obtained through an iterative process that successively refines an initial guess to a solution that is within an acceptable tolerance of the exact solution (ANSYS, 2015). In this analysis, the default solver (Sparse Direct) was used as recommended by the ANSYS manual, (2015) .

Conversions criteria

The ANSYS software iterates the equilibrium equations until the convergence criteria are achieved or until the maximum number of equations is reached. The default convergence criteria in the ANSYS is based on the force convergence criteria; however, you still have the choice to define your convergence criteria based on moments, displacements, or rotations, or any combination of these items. ANSYS checks the convergence criteria by comparing the square root sum of squares of the applied load or displacement against the specified criteria after each load step, if the square root sum of squares is greater than the input value, a new iteration will be processed, and if the square root sum of squares is less than the input value, the ANSYS will step to the next load step. In this study, the default force and displacement criteria were used. However, after the concrete cracked, convergence for the non-linear analysis was impossible with the default values, the force criteria were dropped, and the default values for the displacement criteria were changed to reasonable values that can avoid the convergence problem. Table 4 shows the values of the displacement criteria used for this analysis.

Table 4: Displacement convergence criteria

Item	Value
Reference Value	10
Tolerance	0.05

Results and Discussion

The results from the finite element model were compared against the experimental results found (Palmer, 2010) 8 to verify the method by which the finite element model was built and to verify the software used in the analysis. The verification was based on comparing failure modes, compressive strains, cracking and ultimate loads, and deflection of the poles from the finite element model against the experimental results.

Failure Modes

ANSYS failure modes for the two poles were different. For the first pole, with 6 bars, the two GFRP bars at the bottom side reach an ultimate tensile strain of 0.0169 at the ground line. There was no crushing of concrete reported by ANSYS. However, during the test, the pole crushed at the ground line. On the other hand, for the second pole, with twelve bars, crushing of concrete was observed at the ground line for the ANSYS model and during the test. The tensile strain reported by ANSYS was 0.013 at the ground line.

The equivalent compressive strains during failure are discussed in the following section.

Compressive Strains

Table 5 compares the failure compressive strain at the support from the experimental data with the results from the finite element model for the two poles. It could be seen that the finite element model overestimated the compressive strain at failure for the two poles. For the first pole, with 6 bars, the compressive strain from the finite element model was higher than the experimental compressive strain by 32.4%. This difference between the experimental and the ANSYS results might be contributed to the uncertainty of concrete presented in the difference between the actual and assumed cross-section dimensions, concrete cover, pole orientation during the test, and spinning effect on the compressive strength of concrete. Also, since the poles were manually loaded, the rate of loading is considered another source of uncertainty.

For the second pole, with twelve bars, there was an increase of 9.95% in the finite element model compressive strain at failure load.

Table 5: Experimental and finite element model strain at failure load

Specimen ID	Experimental Loads (Micro strain)	Finite Element Loads (Micro strain)	% Difference
P01	2049	2713	32.4
P02	2402	2641	9.95

Cracking and Ultimate Loads

Table 6 shows the cracking loads predicted by the ANSYS compared to the cracking loads recorded during the test. This table shows that the ANSYS closely estimated the value for the cracking load with a difference of 0.5% for the first pole. However, for the second pole, there was a difference of 6.43% between the ANSYS and the experimental cracking loads.

A comparison between the failure load predicted by the ANSYS and the failure load recorded during the test is shown on Table 7. The ANSYS failure loads are the last applied load steps before the solution diverges and the program terminates. It could be seen from this table that the difference between the ANSYS failure load and the experimental failure load is 5.0% and 0.14% for the first and second poles, respectively.

Table 6: Experimental and finite element model cracking loads

Specimen ID	Experimental Loads (lbs)	Finite Element Loads (lbs)	% Difference
P01	595	598	0.50
P02	653	611	-6.43

Note: 1lbs = 4.45 N

Table 7: Experimental and finite element model failure loads

Specimen ID	Experimental Loads (lbs)	Finite Element Loads (lbs)	% Difference
P01	2980	2834	-5.0
P02	3573	3578	0.14

Note: 1lbs = 4.45 N

Deflection

The load deflection curves for the two poles are shown in Figure 7 and Figure 8, and the tip deflection at experimental failure load is presented in Table 8. In general, the ANSYS results agree quite well with the experimental records. For the second pole, it could be seen in Figure 8 that the ANSYS curve was slightly stiffer than the experimental curve, and this might be due to the difference in the actual modulus of elasticity of concrete for this pole and that used in the ANSYS model. It can also be seen from these figures and from Table 8 that the ANSYS underestimates the tip deflection of the pole at failure, with percentages of 6% and 14.8% for the first and the second poles, respectively. This could be due to two reasons, the first is the way the ANSYS calculates the effective moment of inertia for the poles, and the second is the assumption of a perfect bond between the concrete and the GFRP bars.

Table 8: Experimental and finite tip deflections at failure load

Specimen ID	Experimental [in]	Finite Element Model [in]	% Difference
P01	27.95	26.22	-6.0
P02	25.65	21.84	-14.8

Note: 1in = 25.4 mm

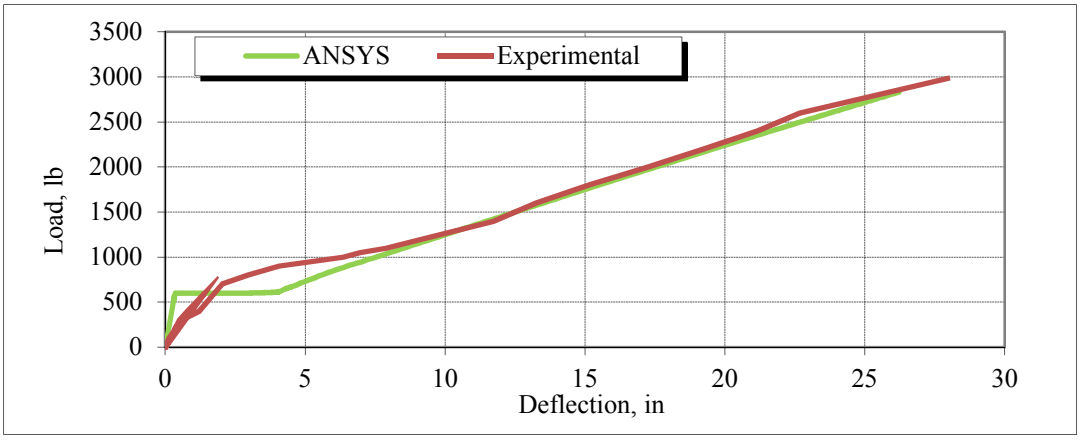

Fig. 7: Load-deflection curve for the first pole
Note: 1in = 25.4 mm 1lbs = 4.45 N

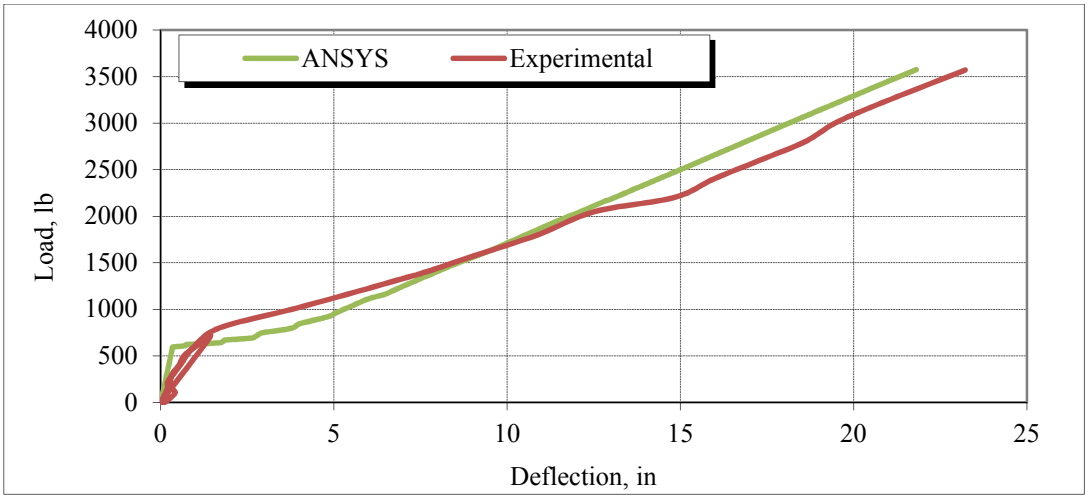

Fig. 8: Load-deflection curve for the second pole
Note: 1in = 25.4 mm 1lbs = 4.45 N

Summary and Conclusion

This study aims to investigate the possibility of modeling spun concrete poles reinforced with GFRP bars using finite element software. Two poles have been modeled using the ANSYS software and the results were compared to the experimental results of two similar poles tested under cantilever load. The conclusions drawn out from this study can be summarized as follows:

In general, the finite element model developed can be used for further studies regarding spun concrete poles reinforced with GFRP bars.

The finite element model was able to predict the flexural behavior of spun concrete poles reinforced with GFRP bars.

The finite element model overestimated the compressive strain values of spun concrete poles reinforced with GFRP bars when compared to the experimental values.

Failure loads of the finite element model compared well with that obtained from the experimental data.

The load deflection curve predicted using the finite element model was well compared to the experimental data.

References

ANSYS, 2015. Release 16.1 Finite Element Analysis System, SAS IP, Inc.

Barbosa, A. F. and G. O. Ribeiro, 1998. Analysis of Reinforced Concrete Structures Using ANSYS Nonlinear Concrete Model. Proceedings, Computational Mechanics, New Trends and Applications, CIMNE, Barcelona, Spain.

Kachlakev, D. I., T. Miller, S. Yim, K. Chansawat and T. Potisuk, 2001. Finite Element Modeling of Reinforced Concrete Structures Strengthened with FRP Laminates." California Polytechnic State University, San Luis Obispo, CA and Oregon State University, Corvallis, OR for Oregon Department of Transportation, May. pp.99

Nawy, E. G., 2000. Fundamentals of High Performance Concrete" 2nd Edition, Wiley, New York.

Nunez, E., 2002. Development of A Flaminated Finite Element for the Analysis of Prestressed Concrete Poles. Ph.D. Dissertation, University of Alabama at Birmingham

Palmer, Sally G., 2010. Flexural Behavior of Spun Concrete Poles Reinforced with Glass Fiber Reinforced Polymer (GFRP)" M.SC. Thesis, University of Alabama at Birmingham.

Willam, K. J. and E. P. Warnke, 1974. Constitutive Model for Triaxial Behavior of Concrete. Seminar on Concrete Structures Subjected to Triaxial Stresses, International Association of Bridge and Structural Engineering Conference, Bergamo, Italy, pp.174

Notations

ε	Strain at any stress f
ε_0	Concrete peak strain in compression
E_c	Modulus of elasticity of concrete
f	Stress at any strain ε
$f_c^{'}$	Cylinder compressive strength of concrete at 28 days
w	Unit weight of concrete in lb/in^3